Materials Science in Semiconductor Processing 204 (2026) 110293

Contents lists available at ScienceDirect

Materials Science in Semiconductor Processing

journal homepage: www.elsevier.com/locate/mssp

Topographically-guided van der Waals epitaxy: Selective growth of AlN nanowalls on h-BN step edges

Albert M. Dautov [a,b], Vladimir G. Dubrovskii [b], Talgat Shugabaev [a,b], Vera V. Lendyashova [a,b], Konstantin P. Kotlyar [a,b,c], Alexey Kuznetsov [e], Prokhor A. Alekseev [f], Mikhail E. Popov [f], Igor V. Shtrom [c], Adilet Toksumakov [g], Davit Ghazaryan [d], Alesya V. Parfeneva [f], Aleksey V. Arsenin [e,g], Alexey D. Bolshakov [b,d,e], George E. Cirlin [a,b,c], Vladislav O. Gridchin [a,b,c,*]

[a] Lab of Epitaxial Nanotechnologies, Alferov University, St. Petersburg, Russia
[b] Faculty of Physics, St. Petersburg State University, St. Petersburg, Russia
[c] Institute for Analytical Instrumentation RAS, St. Petersburg, Russia
[d] Laboratory of Advanced Functional Materials Yerevan State University, Yerevan, Armenia
[e] Moscow Centre for Advanced Studies, Moscow, Russia
[f] Ioffe Institute, St. Petersburg, Russia
[g] Emerging Technologies Research Centre, XPANCEO, Dubai, United Arab Emirates

ARTICLE INFO

Keywords:
AlN
van der Waals epitaxy
h-BN
Two-dimensional materials
Nanowires
Nanowalls
Selective growth

ABSTRACT

Precise spatial and morphological control in the synthesis of semiconductor nanostructures remains a critical challenge for the bottom-up fabrication of integrated nanosystems. Here, we demonstrate that the substrate topography can be used to deterministically control the van der Waals epitaxy of AlN nanostructures on hexagonal boron nitride (h-BN) flakes. Atomic force and scanning electron microscopy studies reveal that vertical AlN nanowires grow randomly on the h-BN surface, while nanowalls preferentially nucleate and propagate along the step edges of h-BN flakes. This morphological selectivity is governed by a critical step height: nucleation of nanowalls occurs only at the steps exceeding a height of 5 ± 1 monolayers of h-BN. In the temperature range from 810 to 850 °C, increasing the growth temperature reduces the nanowire surface density and simultaneously enhances vertical growth of both nanowires and nanowalls. These trends are discussed within a qualitative model. This work establishes a new principle for topographical control over vdW epitaxy, opening a pathway for the fabrication of integrated deep-ultraviolet photonic circuits and ordered piezoelectric nanosystems.

1. Introduction

Aluminum nitride (AlN), with its ultra-wide direct bandgap of approximately 6 eV, stands as the cornerstone semiconductor for optoelectronic devices operating in the deep-ultraviolet (DUV) spectral range [1]. The development of efficient, compact, and robust DUV light sources and detectors is critical for a host of transformative applications, including water purification, surface sterilization, medical diagnostics, and non-line-of-sight communications [2]. However, the performance of conventional planar AlN-based devices is fundamentally hampered by profound materials science challenges [2]. Nanostructures, particularly nanowires (NWs) [3], together with van der Waals (vdW) and remote epitaxy [4] have emerged as powerful platforms to circumvent these limitations. In particular, vdW-based epitaxial growth on two-dimensional material layers offers a promising route for synthesizing high-quality III-nitride nanostructures. The vdW epitaxy is characterized by the weak vdW forces at the growth interface and consequently weak epitaxial constraints [5–7]. Hence, this growth can eliminate residual strain in epitaxial layers and fully circumvent the lattice-mismatch issues, which is crucial for fabricating high quality nanomaterials for efficient optoelectronic devices [8,9]. The vdW epitaxy enables, for example, customizable quantum dots (QDs) with optimal morphology and without any wetting layer between the dots, with is inherent in the Stranski-Krastanov growth mode [10].

* Corresponding author. Lab of Epitaxial Nanotechnologies, Alferov University, St. Petersburg, Russia.
E-mail address: gridchin@spbau.ru (V.O. Gridchin).

https://doi.org/10.1016/j.mssp.2025.110293
Received 12 September 2025; Received in revised form 18 November 2025; Accepted 21 November 2025

Furthermore, it enables transfer of epitaxial layers or nanostructures onto foreign substrates or templates, providing opportunities for heterogeneous integration of III-nitride semiconductors with silicon substrates [10].

Among common 2D materials, hexagonal boron nitride (h-BN) is of particular interest for III-N epitaxy due to its dangling-bond-free surface, exceptional stability at high temperatures [11], wide bandgap (~6 eV) [12] and compatible honeycomb crystal lattice. Unlike graphene, its insulating nature and greater thermal stability make it an ideal substrate and dielectric layer for high-temperature, high-power electronic and optoelectronic devices [13]. The combination of these properties with the tunable direct bandgap of III-nitrides (from 0.7 eV to 6.1 eV) [14] makes this material system highly promising for fabricating efficient light-emitting diodes. In particular, h-BN has shown promise as a p-doped material suitable for fabrication of AlN-based LEDs with the internal quantum efficiency reaching 80 % [15].

Recent progress in vdW epitaxy has led to successful demonstrations of III-V NW growth on 2D virtual substrates, including InAs on h-BN [16] and GaN on graphene [17], typically yielding vertically aligned but randomly distributed NW ensembles. While these results confirm the viability of the approach, the field is now transitioning from proof-of-concept demonstrations to the engineering of functional nanosystems. This transition hinges on overcoming a critical, unaddressed challenge: achieving precise, deterministic control over the morphology and spatial placement of individual nanostructures.

Pioneering work in other material systems, such as the growth of ZnO nanowalls on plasma-treated or artificially ledged h-BN, has highlighted the potential of substrate engineering to guide nucleation [13]. Despite the previously reported NWs and nanowalls (NWLs) growth on graphene layers [18], a method for achieving such architectural control of non-planar III-nitride nanostructures synthesized via the vdW epitaxy remain largely unexplored.

In this work, we demonstrate direct growth of vertical AlN NWs and NWLs by vdW epitaxy on h-BN flakes transferred onto SiO_x/Si substrates. Our study reveals that while NWs nucleate randomly on the flat h-BN terraces, the NWLs nucleate exclusively along the step edges of h-BN flakes, and the step height is found to be the critical parameter for the NWL formation. The study shows that the surface density of AlN structures can be controlled with the growth temperature. These findings are discussed within a qualitative theoretical framework. Crucially, we leverage this fundamental understanding to show that AlN NWLs preferentially nucleate along the step edges of h-BN flakes, enabling patterned growth of AlN on van der Waals surface. This is evidenced by the selective epitaxy of NWLs on lithographically patterned h-BN and points toward the fabrication of efficient optical resonators. These findings shed more light on the formation mechanisms of highly anisotropic AlN nanostructures during the vdW epitaxy on h-BN flakes. The results are promising for synthesis of high-quality III-nitride structures for deep ultraviolet [19] and visible [20] light sources as well as piezoelectric nanosystems on 2D material platforms.

2. Experimental procedures

Growth experiments were carried out in a Riber Compact 12 plasma-assisted molecular beam epitaxy (PA-MBE) setup. Prior to the growth, n-type Si(111) substrates were thermally oxidized using the method reported in Ref. [21], which led to the formation of a 65 nm thick layer of SiO_x. Next, h-BN flakes (2D Semiconductors) were mechanically exfoliated and transferred to the oxide layer. The substrate with the h-BN flakes was then washed in deionized water for 30 s, loaded into the growth chamber and annealed at $T = 850$ °C (as measured by an Optris CT Laser 3MH1 pyrometer) for 15 min. The washing and annealing were used to remove contaminations or salts that may have been introduced during the exfoliation and transfer processes, without the use of aggressive chemicals or sonication that could damage the flakes. Next, the Al shutter was opened to deposit several MLs of Al onto the substrate. Then, the Al shutter was closed and the nitrogen (N) plasma source was initiated. The N flow rate and plasma source power were 0.2 sccm and 350 W, respectively. After stabilization of pressure in the growth chamber, the Al shutter was opened again, and the AlN growth was carried out for 2 h. The beam equivalent pressure of Al flux was 8.4×10^{-8} Torr, as measured prior to the growth using a Bayard-Alpert gauge positioned near the substrate surface. The growth was carried out under nitrogen-rich conditions. The sample surface was monitored in situ using a reflection high-energy electron diffraction (RHEED) system. After the growth, the RHEED diffraction pattern exhibited rings originating from disordered parasitic AlN structures on the oxide surface, and 3D features originating from the wurtzite AlN nanostructures on h-BN flakes.

Morphology properties of AlN nanostructures were studied using a Carl Zeiss Supra 25 SEM system, equipped with an Ultima 100 energy dispersive X-ray analyzer (Oxford Instruments). The h-BN flake location on the SiO_x/Si substrate was identified using a semi-automatic high-resolution optical microscope (Leica INM 100). Raman spectra were acquired using a Horiba Jobin-Yvon LabRAM HR800 spectrometer with a 532 nm laser source. A topography mapping and friction lithography of h-BN flakes were performed using an Ntegra AURA (NT-MDT, Russia) atomic force microscope (AFM) operated in a contact mode. Nanopatterning was performed using commercial scanning probe microscope with a maximum probe moving speed of 400 μm/s. However, in a frictional lithography, there are no physical limitations on reducing the interaction time between the probe and the surface. Thus, specially designed scanning probe lithographs with high-speed scanners employing a multi-probe scheme could enable wafer-scale patterning [22].

3. Results and discussion

Fig. 1 shows typical optical and SEM images of h-BN flakes transferred onto the SiO_x/Si substrate. The lateral size of the flakes ranges from 10 to 200 μm, and the average thickness varies from 50 to 100 nm.

Fig. 2a shows typical SEM image of the grown AlN nanostructures, revealing three distinct morphologies: (i) well-aligned vertical AlN NWs and (ii) NWLs formed on h-BN flakes, and (iii) parasitic AlN nanostructures grown on bare SiO_x surface without h-BN flakes. For clarity, Fig. 2b illustrates an artistic impression of the observed morphologies. The NWs exhibit an average height and diameter of 230 nm and 50 nm, respectively. The NWLs exhibit an average height and width of 205 nm and 40 nm, respectively. Both types of structures exhibit predominantly coherent vertical growth along the c-axis of the wurtzite crystal structure, in contrast to the disordered growth observed on bare SiOx surface. This result may provide a viable route for the growth of continuous AlN thin films on amorphous substrates such as SiO_x, mediated by h-BN

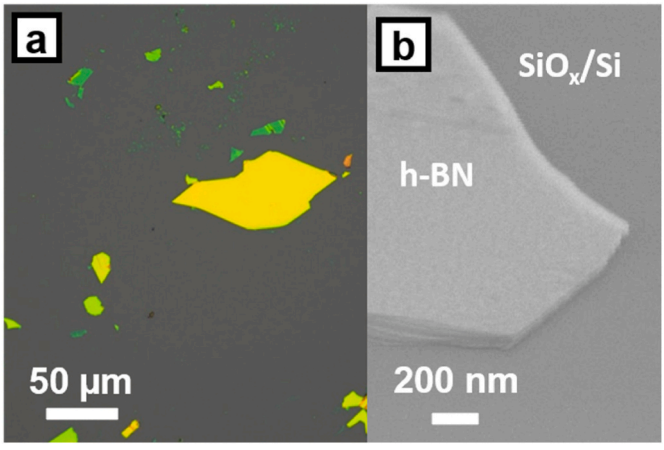

Fig. 1. (a) Optical microscopy and (b) SEM images of h-BN flakes transferred onto the SiOx/Si substrate.

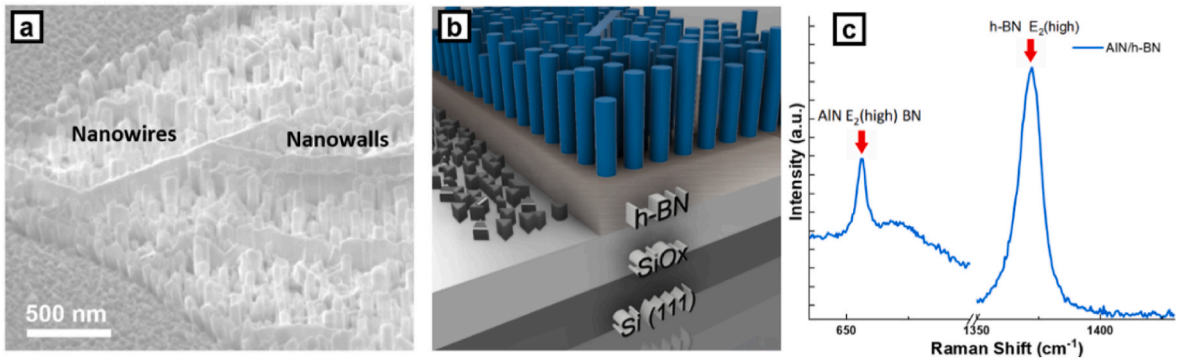

Fig. 2. (a) SEM image of AlN NWs and NWLs on h-BN flake and parasitic structures on SiOx layer. (b) Schematic illustration of the observed morphologies. (c) The Raman spectrum from AlN nanostructures.

layers. The presence of a small fraction of inclined or even horizontally aligned NWs can be due to the ledges or kinks in the h-BN flakes resulting in random growth directions [23].

Fig. 2c shows typical Raman spectra of AlN nanostructures grown on an h-BN flake. The spectrum demonstrates a peak at ~656 cm^{-1} that corresponds to the E_2 high-frequency mode of wurtzite AlN [24]. The observed peak position is consistent with that reported at 655 cm^{-1} for unstrained AlN layers [25]. The full width at half maximum (FWHM) of the E_2(high) mode is only 4.38 cm^{-1}. This very narrow FWHM indicates a high crystal quality of the grown AlN nanostructures. This manifests the advantages of the vdW epitaxy on 2D layered materials [26]. The absence of any dangling bonds in h-BN layer prevents the adatom pinning, thus minimizing the influence of the AlN/h-BN lattice mismatch on the crystal structure of AlN. We also observed the Raman scattering lines in the range from 939 to 978 cm^{-1} (not shown in Fig. 3 c). These lines were previously reported for both SiO_x layer and h-BN flakes in the β-Si_3N_4 (E_{2g}) phase [27]. The observed β-Si_3N_4 phase most probably originates from the plasma activated nitrogen species that react with free Si atoms released from SiO_x at a high surface temperature of 850 °C. The high-energy phonon peak of the Raman spectrum at 1364 cm^{-1} corresponds to the E_{2g} mode of h-BN [28].

To understand the formation mechanisms of different AlN nanostructures, we carefully analyze the surface morphology of an individual h-BN flake before the growth (see Fig. 3a). A multilayer h-BN structure was identified on the selected flake, and the AFM scanning was performed in this region (see Fig. 3b). We can see considerable thickness variation along the flake surface with step edges labeled *a* to *d* in Fig. 3b. Fig. 3c shows the corresponding height profile scans measured across edges *a* to *c* and across a wrinkle *d*. The height measurements were taken at 15 points for each profile. As seen in Fig. 3c, the step heights are 1 nm for step a, 1.8 nm for step b, and 3.9 nm for step c. These values correspond to 3 ± 1, 5 ± 1, and 12 ± 1 MLs of h-BN respectively based

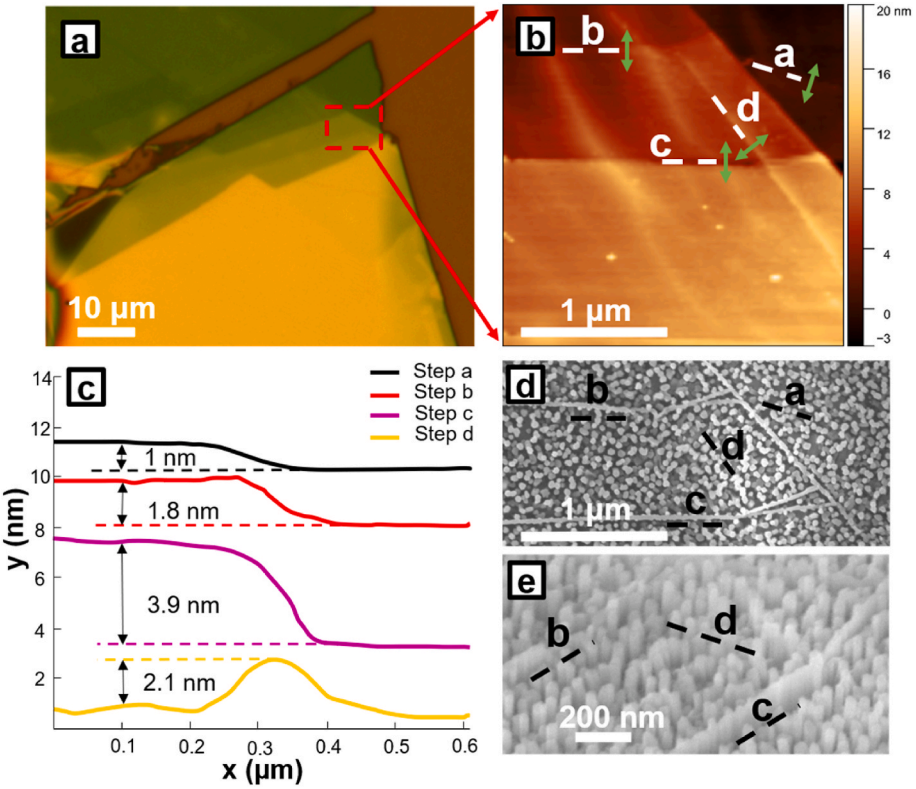

Fig. 3. (a) Optical image of the selected h-BN flake. (b) AFM image of the selected area on the h-BN flake with the marked edges between h-BN layers of different thickness. (c) Height profiles extracted along the line segments indicated in (b). (d–e) Plan-view and cross-section SEM images of the selected area after growth. The indicated line segments are the same as in (b).

on the known ML height of 0.33 nm [29]. The wrinkle *d* height is about 2.1 nm.

This sample was used for the growth of AlN nanostructures. It was found that the NWLs grew exclusively at the high steps. As seen in Fig. 3b–e, the NWLs do not emerge from 3 to 4 ML-high steps. Whereas higher steps (5 MLs and above) provide favorable conditions for NWL nucleation (see Fig. 3d and e). Wrinkles have no dangling bonds, and do not produce any NWLs. For example, no NWL nucleated from the wrinkle *d* having height about 2.1 nm. Therefore, the step height serves as the critical parameter governing the probability of NWL nucleation. Formation of NWLs requires a step to be above the critical height of ~5 MLs of h-BN and is not much influenced by its direction or length.

4. Effect of substrate temperature

To study the temperature effect on the morphology of AlN nanostructures, we grew a series of samples on similar substrates varying only the substrate temperature T while keeping all other conditions identical. Fig. 4a–c shows the SEM images of AlN structures on h-BN flakes obtained at $T = 810$, 830, and 850 °C. We then performed the statistical analysis of these SEM images to determine the surface density of NWs and heights of both NWs and NWLs. These results are shown in Fig. 4d.

As *T* increases in the studied temperature range, the surface density of NWs decreases almost twice, from 3.5×10^9 cm^{-2} at 810 °C to 1.9×10^9 cm^{-2} at 850 °C. At the same time, the average NW height increases by approximately 45 nm. The average height of NWLs also increases by approximately 40 nm. One reason for these trends may be the enhanced nucleation rate of AlN NWs and faster diffusion of Al adatoms along the step at elevated temperatures, resulting in their coalescence into NWLs [30]. The enhanced coalescence process along the step edges may reduce the surface density of NWs, but does not fully explain the increase of their heights. To get more details, we have established a qualitative model of the growth process that is described in the next section.

5. Growth mechanism

According to the experimental data, most AlN structures on h-BN flakes are vertically aligned. Anisotropic growth in the form of self-induced NWs is well-known for MBE of GaN on amorphous SiN_x interlayers on Si(111) substrates under N-rich conditions, and is driven by surface energetics [31]. GaN NWs emerge from isotropic 3D islands. Anisotropic growth starts at a critical island size of about 5 nm, after which the average NW height *H* increases faster than the radius $R \propto H^{\alpha}$, with $\alpha < 1$ [31]. We assume a similar nucleation mechanism for AlN NWs on the surface of h-BN flakes. However, our growth process is complicated by the presence of steps of different heights on the surface. Step edges are known to facilitate spatial inhomogeneity in group III adatom concentration and the corresponding height inhomogeneity in selective area epitaxy of GaN [32,33] and GaAs [34] due to the Ehrlich–Schwoebel barriers for adatom diffusion across the steps. We assume that smaller steps (below the critical height of ~5 MLs of h-BN) do not much influence homogeneous distribution of Al adatoms on the flakes, leading to homogeneous nucleation of AlN NWs illustrated in Fig. 5a. Larger steps above the critical height create the diffusion barrier, which is why the adatom concentration along the step is highest. Surface diffusion flux is also directed along the steps. A combination of these effects leads to preferential nucleation of NWs along the steps, with subsequent coalescence into the NWLs, as illustrated in Fig. 5b. The critical height may depend on temperature due to temperature-activated diffusion of Al adatoms [35–37], but remains approximately constant in the narrow temperature range from 810 °C to 850 °C studied here. Typical growth conditions for AlN NWs in PA-MBE lie in the range of 900–1200 °C [38,39], governed by the low diffusion of Al adatoms. Therefore, within our temperature range, the critical height can be considered approximately constant. At lower temperatures (below 810 °C), the diffusion of Al adatoms during AlN NW growth becomes insufficient, and no growth selectivity is observed. The highest temperature employed in our experiments is limited by the substrate heater. Too high temperatures would lead to enhanced desorption of Al adatoms from the surface and the corresponding growth suppression [35]. We do not see any other explanation of the NWL formation rather than the effect of step edges on surface diffusion of Al adatoms in an optimal temperature range. A more detailed analysis of the critical height versus the growth parameters and the technique of flake preparation requires additional studies and will be presented elsewhere. Our semi-qualitative model remains valid for any critical height.

Nucleation and growth of AlN NWs occurs under constant material flux. In this case, the surface density should decrease with temperature

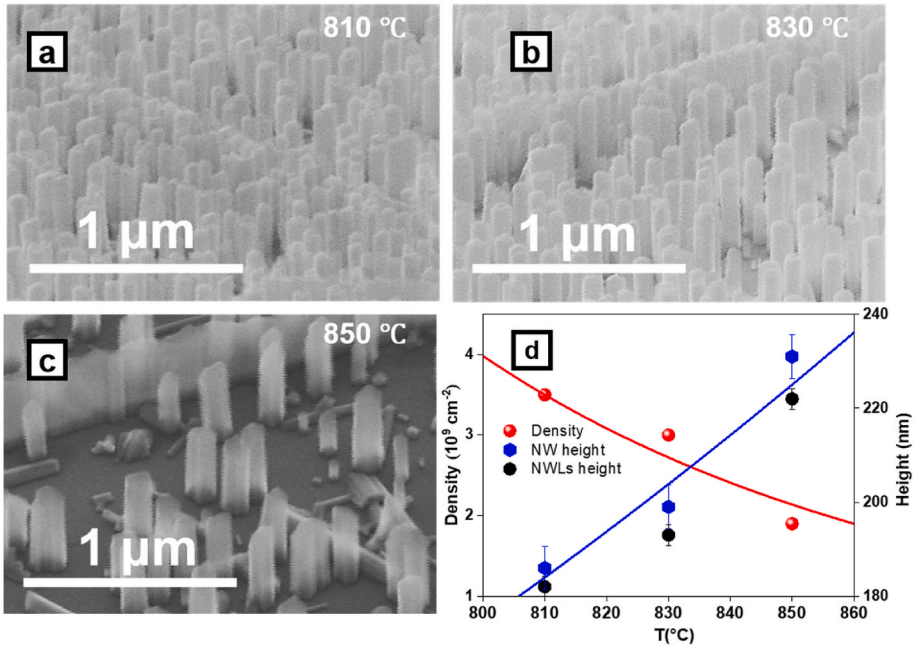

Fig. 4. SEM images of AlN nanostructures grown at (a) 810 °C, (b) 830 °C, and (c) 850 °C. (d) Temperature dependence of the morphological parameters of NWs and NWLs, obtained from the statistical analysis of SEM images in (a), (b) and (c) (symbols). Lines show the Arrhenius fits by the model.

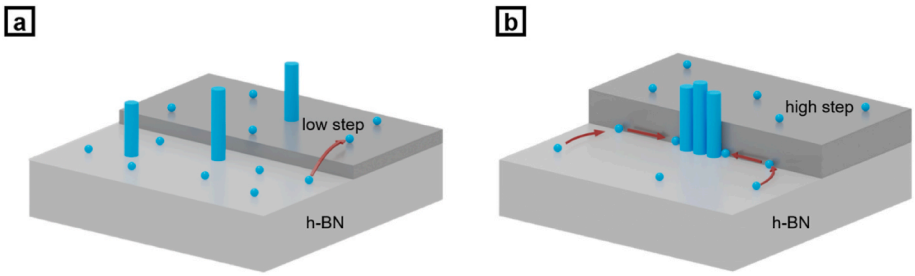

Fig. 5. Illustration of (a) spatially homogeneous nucleation of AlN NWs near low steps and (b) preferential nucleation along high steps, with subsequent coalescence of NWs into NWLs.

according to the general growth theory [40]. This effect, confirmed experimentally for different self-induced III-V nanostructures [40] including InAs/GaAs Stranski-Krastanov islands [41], originates from the kinetically controlled growth conditions for surface nanostructures. In the kinetically controlled regime, the density N exponentially decreases with temperature and increases as a power low function of flux. The average size increases with temperature and the amount of material and decreases with flux [40]. At a fixed flux and deposition thickness h, we can use $N \propto \exp\left(E/k_BT\right)$, with an activation energy E. Assuming $h \cong N\pi R^2 H$ for all temperatures in the investigated range and using $R \propto H^{\alpha}$, we obtain $H \propto N^{-1/(2\alpha+1)} \propto \exp\left[-E/(2\alpha+1)k_BT\right)$. Lines in Fig. 4d show the reasonable fits to the data, obtained from these expressions at $E = 1.29$ eV and $\alpha = 0.72$. More systematic investigations of the growth mechanisms require time-dependent measurements under different temperatures, Al fluxes, and surface preparation techniques, which will be presented elsewhere.

6. Patterned growth of AlN NWLs

As shown earlier, AlN NWLs preferentially grow along the high steps of h-BN flakes. Such steps can be formed deliberately via surface patterning [42]. To demonstrate this, we preliminary patterned a selected h-BN flake using frictional scanning probe lithography in an AFM setup, as described in Refs. [43,44]. Fig. 6a shows an optical image of the patterned flake. During the lithography process, we fabricated a series of the nearly concentric circles by applying sufficient force to cut the flake and form additional step edges. The local over-pressuring resulted in partial flake delamination, seen in Fig. 6a. The growth of AlN was then carried out at $T = 850$ °C. Fig. 6b shows the SEM image of the h-BN flake after the growth process. Fig. 6c shows the magnified SEM image of a smaller surface area marked in Fig. 6b. From Fig. 6c, it is evident that the lithographic patterning of steps initiates the NWL growth, which is clearly observed in the marked areas. The formation of multiple parallel NWLs is also observed, and explained by multiple passes of the AFM probe at the lithographic step. Therefore, the lithographic patterning of the h-BN flakes largely increases the number of AlN NWLs. Although the process is not fully optimized, the results establish a new principle for topographical control over vdW epitaxy.

7. Conclusions

In summary, this study demonstrates the vdW MBE growth of AlN NWs and NWLs on h-BN flakes. These AlN nanostructures exhibit high crystal quality, as confirmed by Raman spectroscopy with a narrow E_2(high) phonon mode (FWHM = 4.38 cm^{-1}). The NWLs preferentially nucleate along the step edges of h-BN flakes when the step height exceeds the critical value of ~5 ML of h-BN. This facilitates the NWL formation on the friction-lithography-patterned h-BN surfaces. The temperature increase from 810 °C to 850 °C leads to the two-fold decrease in the surface density and the simultaneous increase in the height of both NWs and NWLs. The observed trends are explained within a qualitative model. The NWL formation along the high steps is attributed to the diffusion barrier for Al adatoms that facilitates nucleation of dense NWs near the steps and their subsequent coalescence into NWLs due to radial growth. Temperature dependence of the surface density and height of the nanostructures is explained by the kinetically driven growth mode.

These results shed more light on the formation mechanisms of highly anisotropic AlN nanostructures on h-BN. The protocols may be further optimized to yield more regular nanostructures in the selective epitaxy

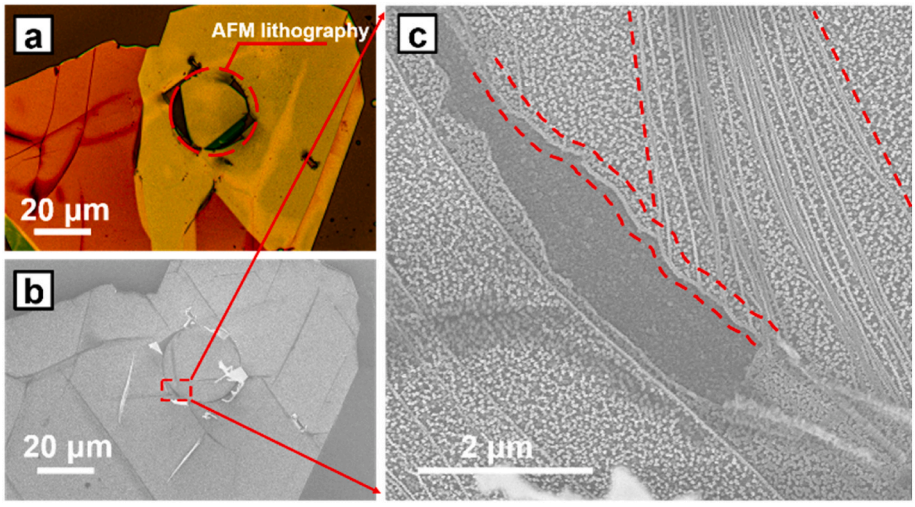

Fig. 6. (a) Optical image of the selected h-BN flake region after lithographic patterning. (b) SEM image of the selected flake region after growth of AlN. (c) Magnified SEM image of the selected flake region, where multiple NWLs formed in the areas marked by dashed lines.

approach, and translated to other material systems such as In(Ga)N compounds.

CRediT authorship contribution statement

Albert M. Dautov: Writing – original draft, Visualization, Investigation. **Vladimir G. Dubrovskii:** Writing – review & editing, Methodology, Funding acquisition, Formal analysis, Conceptualization. **Talgat Shugabaev:** Visualization, Validation, Investigation. **Vera V. Lendyashova:** Visualization, Software, Investigation, Data curation. **Konstantin P. Kotlyar:** Visualization, Validation, Investigation. **Alexey Kuznetsov:** Validation, Investigation. **Prokhor A. Alekseev:** Writing – review & editing, Visualization, Validation, Investigation, Conceptualization. **Mikhail E. Popov:** Validation, Investigation. **Igor V. Shtrom:** Validation, Software, Investigation. **Adilet Toksumakov:** Resources, Investigation. **Davit Ghazaryan:** Validation, Investigation. **Alesya V. Parfeneva:** Resources, Investigation. **Aleksey V. Arsenin:** Validation, Investigation. **Alexey D. Bolshakov:** Writing – review & editing, Validation, Project administration, Conceptualization. **George E. Cirlin:** Writing – review & editing, Validation, Funding acquisition, Formal analysis, Conceptualization. **Vladislav O. Gridchin:** Writing – original draft, Supervision, Investigation, Conceptualization.

Declaration of competing interest

The authors declare that they have no known competing financial interests or personal relationships that could have appeared to influence the work reported in this paper.

Acknowledgements

Growth experiments were carried out with financial support of the Russian Science Foundation (Project No. 23-79-00012). The study of morphological properties using scanning electron microscopy was carried out with the financial support of the Ministry of Science and Higher Education of the Russian Federation, IAP RAS No. 075-00444-25-00 (FFZM-2025-0004). V.G.D. gratefully acknowledges St. Petersburg State University (research project No. 129360164) for financial support of modeling. A topography mapping and friction lithography of h-BN flakes were performed with financial support of the Russian Science Foundation (Project No. 24-12-00209). A.D.B. acknowledges Russian Science Foundation (Grant 24-12-00225) for support of substrate preparation. The study of structural properties using Raman spectroscopy was conducted with the support of the Ministry of Science and Higher Education of the Russian Federation (State task No. 0791-2023-0004).

Data availability

Data will be made available on request.

References

[1] A.L. Hickman, R. Chaudhuri, S.J. Bader, K. Nomoto, L. Li, J.C. Hwang, H.G. Xing, D. Jena, Next generation electronics on the ultrawide-bandgap aluminum nitride platform, Semicond. Sci. Technol. 36 (2021) 044001.

[2] S. Zhao, A. Connie, M. Dastjerdi, X. Kong, Q. Wang, M. Djavid, S. Sadaf, X. Liu, I. Shih, H. Guo, Aluminum nitride nanowire light emitting diodes: breaking the fundamental bottleneck of deep ultraviolet light sources, Sci. Rep. 5 (2015) 8332.

[3] V. Dubrovskii, G. Cirlin, V. Ustinov, Semiconductor nanowhiskers: synthesis, properties, and applications, Semiconductors 43 (2009) 1539–1584.

[4] Y. Wen, J. Ning, H. Wu, H. Zhang, R. Cheng, L. Yin, H. Wang, X. Zhang, Y. Liu, D. Wang, Y. Hao, J. Zhang, J. He, Van Der Waals Integration of 4-Inch Single-Crystalline III-Nitride Semiconductors, Adv. Mater. 37 (2025) 2501916, https://doi.org/10.1002/adma.202501916.

[5] J. Yu, L. Wang, Z. Hao, Y. Luo, C. Sun, J. Wang, Y. Han, B. Xiong, H. Li, Van der Waals epitaxy of iii-nitride semiconductors based on 2D materials for flexible applications, Adv. Mater. 32 (2020) 1903407.

[6] P. Wang, A. Pandey, J. Gim, W.J. Shin, E.T. Reid, D.A. Laleyan, Y. Sun, D. Zhang, Z. Liu, Z. Zhong, R. Hovden, Z. Mi, Graphene-assisted molecular beam epitaxy of AlN for AlGaN deep-ultraviolet light-emitting diodes, Appl. Phys. Lett. 116 (2020) 171905, https://doi.org/10.1063/1.5144906.

[7] H. Chang, Z. Chen, W. Li, J. Yan, R. Hou, S. Yang, Z. Liu, G. Yuan, J. Wang, J. Li, P. Gao, T. Wei, Graphene-assisted quasi-van der Waals epitaxy of AlN film for ultraviolet light emitting diodes on nano-patterned sapphire substrate, Appl. Phys. Lett. 114 (2019) 091107, https://doi.org/10.1063/1.5081112.

[8] A. Dautov, T. Shugabaev, A. Kuznetsov, K. Kotlyar, D. Ghazaryan, A. Toksumakov, A. Bolshakov, A. Parfeneva, G. Cirlin, V. Gridchin, Epitaxial growth of AlN nanowires on two-dimensional h-BN flakes transferred onto SiO2/Si substrate, in: 2025 IEEE 26th International Conference of Young Professionals in Electron Devices and Materials (EDM), 2025, pp. 100–103, https://doi.org/10.1109/EDM65517.2025.11096650.

[9] H. Wu, J. Ning, J. Zhang, Y. Zeng, Y. Jia, J. Zhao, L. Bai, Y. Wang, S. Li, D. Wang, Y. Hao, High quality AlN film assisted by graphene/sputtered AlN buffer layer for deep-ultraviolet-LED, Nanotechnology 34 (2023) 295202, https://doi.org/10.1088/1361-6528/accc39.

[10] J. Jeong, D.K. Jin, J. Choi, J. Jang, B.K. Kang, Q. Wang, W.I. Park, M.S. Jeong, B.-S. Bae, W.S. Yang, Transferable, flexible white light-emitting diodes of GaN p–n junction microcrystals fabricated by remote epitaxy, Nano Energy 86 (2021) 106075.

[11] S. Sundaram, X. Li, Y. Halfaya, T. Ayari, G. Patriarche, C. Bishop, S. Alam, S. Gautier, P.L. Voss, J.P. Salvestrini, A. Ougazzaden, Large-Area van der Waals Epitaxial Growth of Vertical III-Nitride Nanodevice Structures on Layered Boron Nitride, Adv. Mater. Interfac. 6 (2019) 1900207, https://doi.org/10.1002/admi.201900207.

[12] A. Zaiter, A. Michon, M. Nemoz, A. Courville, P. Vennéguès, V. Ottapilakkal, P. Vuong, S. Sundaram, A. Ougazzaden, J. Brault, Crystalline quality and surface morphology improvement of face-to-face annealed MBE-Grown AlN on h-BN, Materials 15 (2022) 8602, https://doi.org/10.3390/ma15238602.

[13] H. Oh, Y.J. Hong, K.-S. Kim, S. Yoon, H. Baek, S.-H. Kang, Y.-K. Kwon, M. Kim, G.-C. Yi, Architectured van der Waals epitaxy of ZnO nanostructures on hexagonal BN, NPG Asia Mater. 6 (2014) e145–e145.

[14] G. Cassabois, P. Valvin, B. Gil, Hexagonal boron nitride is an indirect bandgap semiconductor, Nat. Photonics 10 (2016) 262–266.

[15] D.A. Laleyan, S. Zhao, S.Y. Woo, H.N. Tran, H.B. Le, T. Szkopek, H. Guo, G. A. Botton, Z. Mi, AlN/h-BN heterostructures for Mg dopant-free deep ultraviolet photonics, Nano Lett. 17 (2017) 3738–3743, https://doi.org/10.1021/acs.nanolett.7b01068.

[16] A.G.S. Vilasam, S. Adhikari, B. Gupta, S. Balendhran, N. Higashitarumizu, J. Tournet, L. Li, A. Javey, K.B. Crozier, S. Karuturi, Large-area epitaxial growth of InAs nanowires and thin films on hexagonal boron nitride by metal organic chemical vapor deposition, Nanotechnology 34 (2023) 495601.

[17] V. Kumaresan, L. Largeau, A. Madouri, F. Glas, H. Zhang, F. Oehler, A. Cavanna, A. Babichev, L. Travers, N. Gogneau, Epitaxy of GaN nanowires on graphene, Nano Lett. 16 (2016) 4895–4902.

[18] B. Kumar, K.Y. Lee, H.-K. Park, S.J. Chae, Y.H. Lee, S.-W. Kim, Controlled growth of semiconducting nanowire, nanowall, and hybrid nanostructures on graphene for piezoelectric nanogenerators, ACS Nano 5 (2011) 4197–4204.

[19] T. Makimoto, K. Kumakura, Y. Kobayashi, T. Akasaka, H. Yamamoto, A vertical InGaN/GaN light-emitting diode fabricated on a flexible substrate by a mechanical transfer method using BN, Appl. Phys. Express 5 (2012) 072102, https://doi.org/10.1143/APEX.5.072102.

[20] V.G. Dubrovskii, G.E. Cirlin, D.A. Kirilenko, K.P. Kotlyar, I.S. Makhov, R.R. Reznik, V.O. Gridchin, Instantaneous growth of single monolayers as the origin of spontaneous core–shell in x Ga 1− x N nanowires with bright red photoluminescence, Nanoscale Horiz. 9 (2024) 2360–2367.

[21] L. Dvoretckaia, V. Gridchin, A. Mozharov, A. Maksimova, A. Dragunova, I. Melnichenko, D. Mitin, A. Vinogradov, I. Mukhin, G. Cirlin, Light-Emitting Diodes Based on InGaN/GaN Nanowires on Microsphere-Lithography-Patterned Si Substrates, Nanomaterials 12 (2022) 1993, https://doi.org/10.3390/nano12121993.

[22] R. Garcia, A.W. Knoll, E. Riedo, Advanced scanning probe lithography, Nat. Nanotechnol. 9 (2014) 577–587.

[23] K. Chung, H. Beak, Y. Tchoe, H. Oh, H. Yoo, M. Kim, G.-C. Yi, Growth and characterizations of GaN micro-rods on graphene films for flexible light emitting diodes, APL Mater. 2 (2014).

[24] J.D. Caldwell, I. Aharonovich, G. Cassabois, J.H. Edgar, B. Gil, D.N. Basov, Photonics with hexagonal boron nitride, Nat. Rev. Mater. 4 (2019) 552–567.

[25] V.N. Jmerik, A.N. Semenov, D.V. Nechaev, S.I. Troshkov, D.D. Sakhno, P. A. Alekseev, D.A. Kirilenko, I.A. Eliseyev, V.Yu Davydov, A.S. Abbas, Low-defect and stress-free AlN(0001) nanoprisms and microrods selectively grown on micro-patterned c-sapphire substrate by plasma-assisted molecular beam epitaxy, Appl. Phys. Lett. 124 (2024) 232104, https://doi.org/10.1063/5.0216809.

[26] F. Tiour, B. Benyahia, N. Brihi, A. Sari, B. Mahmoudi, A. Manseri, A. Guenda, Opto-structural properties of Si-rich SiNx with different stoichiometry, Appl. Phys. A 126 (2020) 59.

[27] N. Wada, S. Solin, J. Wong, S. Prochazka, Raman and IR absorption spectroscopic studies on α, β, and amorphous Si3N4, J. Non-Cryst. Solids 43 (1981) 7–15.

[28] R. Arenal, A.C. Ferrari, S. Reich, L. Wirtz, J.-Y. Mevellec, S. Lefrant, A. Rubio, A. Loiseau, Raman spectroscopy of single-wall boron nitride nanotubes, Nano Lett. 6 (2006) 1812–1816, https://doi.org/10.1021/nl0602544.

[29] S. Ali, P.M. Ismail, M. Humayun, M. Bououdina, Hexagonal boron nitride: from fundamentals to applications, Desalination 599 (2025) 118442.

[30] A. Zhong, K. Hane, Growth of GaN nanowall network on Si (111) substrate by molecular beam epitaxy, Nanoscale Res. Lett. 7 (2012) 686, https://doi.org/10.1186/1556-276X-7-686.

[31] V.G. Dubrovskii, V. Consonni, L. Geelhaar, A. Trampert, H. Riechert, Scaling growth kinetics of self-induced GaN nanowires, Appl. Phys. Lett. 100 (2012) 153101, https://doi.org/10.1063/1.3701591.
[32] M.M. Rozhavskaya, W.V. Lundin, S.I. Troshkov, A.F. Tsatsulnikov, V.G. Dubrovskii, Determination of the diffusion lengths of Ga adatoms using GaN stripe profiling, Phys. Status Solidi 212 (2015) 851–854, https://doi.org/10.1002/pssa.201431912.
[33] M. Sobanska, Z.R. Zytkiewicz, M. Ekielski, K. Klosek, A.S. Sokolovskii, V. G. Dubrovskii, Surface diffusion of gallium as the origin of inhomogeneity in selective area growth of GaN nanowires on Al $_x$ O $_y$ nucleation stripes, Cryst. Growth Des. 20 (2020) 4770–4778, https://doi.org/10.1021/acs.cgd.0c00530.
[34] D. Dede, F. Glas, V. Piazza, N. Morgan, M. Friedl, L. Güniat, E. Nur Dayi, A. Balgarkashi, V.G. Dubrovskii, A. Fontcuberta I Morral, Selective area epitaxy of GaAs: the unintuitive role of feature size and pitch, Nanotechnology 33 (2022) 485604, https://doi.org/10.1088/1361-6528/ac88d9.
[35] P. John, M.G. Ruiz, L. van Deurzen, J. Lähnemann, A. Trampert, L. Geelhaar, O. Brandt, T. Auzelle, Growth kinetics and substrate stability during high-temperature molecular beam epitaxy of AlN nanowires, Nanotechnology 34 (2023) 465605.
[36] H. Liu, P. Shao, Y. Liu, Q. Yao, T. Tao, Z. Xie, D. Chen, B. Liu, H. Lu, R. Zhang, A growth diagram of AlN epilayers grown by plasma assisted molecular beam epitaxy, Chin. Phys. B (2025).
[37] I. Bryan, Z. Bryan, S. Mita, A. Rice, J. Tweedie, R. Collazo, Z. Sitar, Surface kinetics in AlN growth: a universal model for the control of surface morphology in III-nitrides, J. Cryst. Growth 438 (2016) 81–89.
[38] Z. Hao, J. Yu, C. Wu, R. Liu, L. Wang, B. Xiong, J. Wang, Y. Han, C. Sun, Y. Luo, MBE growth of AlN nanowires on Si substrates by aluminizing nucleation, Nanoscale Res. Lett. 10 (2015) 1–7.
[39] Ž. Gačević, J. Grandal, Q. Guo, R. Kirste, M. Varela, Z. Sitar, M.S. García, Structural and optical properties of self-assembled AlN nanowires grown on SiO2/Si substrates by molecular beam epitaxy, Nanotechnology 32 (2021) 195601.
[40] V.G. Dubrovskii, Nucleation Theory and Growth of Nanostructures, Springer Berlin Heidelberg, Berlin, Heidelberg, 2014, https://doi.org/10.1007/978-3-642-39660-1.
[41] V.G. Dubrovskii, G.E. Cirlin, V.M. Ustinov, Kinetics of the initial stage of coherent island formation in heteroepitaxial systems, Phys. Rev. B 68 (2003) 075409, https://doi.org/10.1103/PhysRevB.68.075409.
[42] B.R. Borodin, F.A. Benimetskiy, P.A. Alekseev, Study of local anodic oxidation regimes in MoSe2, Nanotechnology 32 (2021) 155304.
[43] B.R. Borodin, F.A. Benimetskiy, V.Yu Davydov, I.A. Eliseyev, A.N. Smirnov, D. A. Pidgayko, S.I. Lepeshov, A.A. Bogdanov, P.A. Alekseev, Indirect bandgap $MoSe_2$ resonators for light-emitting nanophotonics, Nanoscale Horiz. 8 (2023) 396–403, https://doi.org/10.1039/D2NH00465H.
[44] P.A. Alekseev, I.A. Milekhin, K.A. Gasnikova, I.A. Eliseyev, V.Y. Davydov, A. A. Bogdanov, V. Kravtsov, A.O. Mikhin, B.R. Borodin, A.G. Milekhin, Engineering whispering gallery modes in MoSe2/WS2 double heterostructure nanocavities: towards developing all-TMDC light sources, Mater. Today Nano 30 (2025) 100633, https://doi.org/10.1016/j.mtnano.2025.100633.